J. Fluid Mech. (1983), *vol.* 133, *pp.* 297–319
Printed in Great Britain

Effects of rotation and shear on doubly diffusive instability

By SYLVIA WORTHEM,
Sea–Air Interaction Laboratory, NOAA, Miami, Florida

E. MOLLO-CHRISTENSEN AND F. OSTAPOFF
Massachusetts Institute of Technology, Cambridge, Massachusetts
Sea–Air Interaction Laboratory, NOAA, Miami, Florida

(Received 2 June 1982 and in revised form 7 April 1983)

A linear stability analysis of a doubly diffusive system, with rotation and shear, shows that overstable oscillations can occur in stratifications typical of the equatorial ocean, that internal waves encountering an equatorial current can exchange energy with the current, and that the wave-induced fluxes of salt and heat can lead to layer formation in the salinity, temperature and velocity fields.

1. Introduction

If salt and heat are assumed to be passive contaminants of oceanic turbulence, the observed turbulence levels are insufficient to produce the observed distributions of temperature and salinity, as was pointed out by Munk (1966). It is therefore reasonable to surmise that salt and heat play an active role in the generation and dissipation of oceanic turbulence. One mechanism of mixing where heat and salt play active roles is the salt-finger instability proposed by Stern (1960), which has been intensively explored in recent years. Layer formation, rather than smoothing of density stratification, can result from thermohaline instability.

In regions of moderately or highly stable density stratification with low velocity shear, we have to look for mechanisms other than shear mixing to account for the vertical fluxes of salt and heat needed to maintain the observed distributions. Internal waves may provide an intermittent source of shear of sufficient intensity to lower the local Richardson number into the unstable range, as observed by Woods (1968). Regions characterized by high stability and large shear are found mostly in the tropical current system, which has a complex horizontal and vertical structure (Duing, Ostapoff & Merle 1980). We will show that shear and rotation in combination can induce thermohaline instability and cause mixing under conditions that would be otherwise stable. The possible instability of a doubly diffusive system due to such added effects may be important in a wide range of planetary and stellar phenomena, as well as in engineering problems dealing with centrifugal separators and other devices. Thermohaline instability exhibits the important feature that fluctuations in vertical velocity, salinity and temperature are closely correlated. Therefore relatively weak vertical velocities will produce much larger transports than a turbulent velocity field independent of heat and salt.

Our analysis is an extension of previous work on oceanic mixing processes and thermohaline stability, of which we mention the following important contributions.

(i) Baines & Gill (1969) solved the linear thermohaline stability problem for constant vertical gradients of temperature and salinity. They found, in addition to

the salt-finger instability of Stern (1960), the overstable wave instability alluded to by Stommel (1962) and demonstrated experimentally by Turner & Stommel (1964).

(ii) Pearlstein (1981) analysed horizontally propagating disturbances in a rotating doubly diffusive system. He found that rotation affects stability. Schmitt & Lambert (1979) found that rotation tends to stabilize salt-finger perturbations.

(iii) Stern (1969) and Linden (1974) have analysed the effects of shear on salt-finger instability, and found that salt fingers tend to form two-dimensional sheets in a shear flow. Hsu (1974) considered the influence of weak shear on thermohaline instability in general. He determined which modes of instability were preferred in different regimes and whether the heat and salt fluxes were enhanced or inhibited. In a review paper, Huppert & Turner (1981) summarized important applications of doubly diffusive convection theory to geophysical phenomena.

(iv) Stern (1975) and Holyer (1981) showed that thermohaline instability can transfer energy to long internal waves, and thus affect the large-scale field of motion.

(v) Proctor (1981) found that finite-amplitude disturbances could be sustained under conditions where a thermohaline system would be stable to infinitesimal perturbations.

(vi) Maslowe (1974), Siegmann (1974) and Gans (1975) showed that rotation can destabilize shear layers in non-axisymmetric shear flows.

Through the inclusion of variable temperature and salinity gradients, shear and rotation, our analysis extends the above studies and shows that a combination of rotation and shear can destabilize an otherwise stable thermohaline stratification. We describe the stratification in terms of background, mean and perturbation fields in §2. We then formulate a linear perturbation of the mean field in §3, obtain the mean-field equations and linear-perturbation equations in §§4 and 5, obtain the characteristic equation for the planar wave solution in §6, and discuss its roots and their physical significance in §7. In §8 variable shear and variable stratification are considered, in §9 examples of heat, salt, momentum and mass flux calculations are presented, and in §10 oceanographic applications are discussed. The mean-field perturbations considered in §§3–10 can cause disturbances to grow. In §11 we present an analysis that gives the probability distributions of the temperature- and salinity-gradient perturbations for the case of sporadic shear disturbances.

Our analysis follows closely that of Baines & Gill (1969). Thus the effects of rotation and shear on thermohaline diffusion will be apparent. We find that overstable travelling-wave instabilities are possible in the tropical ocean. Our flux calculations show the tendency to layer formation as a result of instability. The horizontal momentum transports suggest that the instabilities we consider can contribute to formation of shear layers and velocity jets. Because lognormal probability densities of normalized salinity and temperature gradient variance have been observed, for example, by Gregg, Cox & Hacker (1973) and by Elliott & Oakey (1980), we describe a process that yields such a probability distribution.

2. Background, mean and perturbation fields

The temperature and salinity fields are described in terms of a uniform background field, a mean stratification, and a time- and space-dependent perturbation field, so that the temperature field T is written as

$$T = T_{\mathrm{b}} + T_{\mathrm{m}}(y, z) + T_{\mathrm{p}}(x, y, z, t) \tag{2.1}$$

and the salinity field S is given by

$$S = S_b + S_m(y,z) + S_p(x,y,z,t). \tag{2.2}$$

Here the subscripts b, m and p refer to background, mean and perturbation respectively. The velocity field $\boldsymbol{V} = (u,v,w)$ is taken to consist of a mean velocity $\bar{U}(z)$, positive towards the east in geophysical applications, and a fluctuating velocity field (u',v',w').

The horizontal lengthscales of the mean and the perturbation fields have to be well separated for the perturbation problem to be formulated as a perturbation on a horizontally quasi-homogeneous mean field. For oceanic applications we identify the mean field with oceanic fine structure and follow Fedorov (1978), who defined the vertical scale of variability of the fine structure to be of the order of one metre and larger. The perturbation field can be identified as the oceanic microstructure field.

3. Formulation of stability problem for constant velocity shear

In our formulation of the problem, we include the effects of both the vertical and horizontal components of the angular velocity of the system as a whole. This is motivated not only by our interest in salt mixing in the equatorial ocean, but also because the local gravitational field is not parallel to the rotation vector in stellar or planetary problems, while, in centrifugal separators, the local acceleration field is nearly normal to the angular velocity. Dowden (1972) found that horizontal rotation was important in the equatorial inertial boundary layer, and Kozlov (1967) reached a similar conclusion for a layer deeper than 500 m, where he found that the horizontal component of the Earth's angular velocity has a significant effect.

Let the angular velocity of the fluid as a whole be $\boldsymbol{\Omega}$, so that it has vertical and horizontal components $\frac{1}{2}f$ and $\frac{1}{2}f_H$, respectively. Using subscripts x,y,z,t for partial derivatives in space and time, the momentum equations are

$$u_t + \boldsymbol{v}\cdot\nabla u - \nu\nabla^2 u - fv + f_H w + \frac{p_x}{\rho} = 0, \tag{3.1}$$

$$v_t + \boldsymbol{v}\cdot\nabla v - \nu\nabla^2 v + fu + \frac{p_y}{\rho} = 0, \tag{3.2}$$

$$w_t + \boldsymbol{v}\cdot\nabla w - \nu\nabla^2 w - f_H u + \frac{g\rho'}{\rho} + \frac{p_z}{\rho} = 0, \tag{3.3}$$

in the x-, y- and z-directions respectively, with velocity (u, v, w), kinematic viscosity ν, pressure p, and density ρ. We have used the Boussinesq approximation, with ρ' denoting the density anomaly, which, in turn, is related to anomalies of temperature $\mathrm{d}T = T - T_b$ and salinity $\mathrm{d}S = S - S_b$ by the equation of state (Veronis 1965)

$$\rho = \rho_b + \rho' = \rho_b(1 - \alpha\,\mathrm{d}T + \beta\,\mathrm{d}S). \tag{3.4}$$

Here α and β are constant coefficients, ρ_b is the background density and $\rho' = \rho_m(y,z) + \rho_p(x,y,z,t)$. Incompressibility requires

$$u_x + v_y + w_z = 0. \tag{3.5}$$

Conservation of heat and salt require that

$$T_t + \boldsymbol{v}\cdot\nabla T - \kappa_T\nabla^2 T = 0, \tag{3.6}$$

$$S_t + \boldsymbol{v}\cdot\nabla S - \kappa_s\nabla^2 S = 0, \tag{3.7}$$

where κ_T and κ_S are the thermal and salt diffusivities, respectively. We have assumed that there are no sources of salt and heat in the interior of the fluid. We use the expressions for temperature and salinity given in (2.1) and (2.2); the velocity field $\boldsymbol{V}$ is decomposed into a mean field $\overline{U}$ and a perturbation field (u', v', w'):

$$\boldsymbol{V} = (\overline{U}(z), 0, 0) + (u', v', w'). \tag{3.8}$$

The pressure field is expressed as a sum of a time-averaged mean field $\bar{p}(x, y, z)$ and a time-dependent perturbation field p':

$$p = \bar{p}(x, y, z) + p'(x, y, z, t). \tag{3.9}$$

4. The mean-field equations

In the absence of perturbations, the momentum equations (3.1)–(3.3) reduce to

$$-\nu\nabla^2\overline{U} + \frac{\bar{p}_x}{\rho_b} = 0, \tag{4.1}$$

$$f\overline{U} + \frac{\bar{p}_y}{\rho_b} = 0, \tag{4.2}$$

$$-f_H\,\overline{U} + g(-\alpha T_m + \beta S_m) + \frac{\bar{p}_z}{\rho_m} = 0, \tag{4.3}$$

and the conservation of heat and salt requires

$$\kappa_T\,\nabla^2 T_m = 0, \tag{4.4}$$

$$\kappa_S\,\nabla^2 S_m = 0. \tag{4.5}$$

These equations describe the mean field seen by the perturbations. The mean-field velocity $\overline{U}$ can be divided into ageostrophic and geostrophic components $\overline{U}_a$ and $\overline{U}_g$ respectively:

$$\overline{U}(z) = \overline{U}_a(z) + \overline{U}_g, \tag{4.6}$$

where the geostrophic current shear and the horizontal density gradient satisfy the thermal wind balance

$$f\overline{U}_{gz} = \frac{g\rho_{my}}{\rho_b}. \tag{4.7}$$

5. The linear perturbation equations

After subtracting (4.1)–(4.5) from (3.1)–(3.7), dropping nonlinear terms and omitting the primes, we obtain the perturbation equations

$$u_t + \overline{U}u_x + w(\overline{U}_z + f_H) - fv - \nu\nabla^2 u + \frac{p_x}{\rho_b} = 0, \tag{5.1}$$

$$v_t + \overline{U}v_x + fu - \nu\nabla^2 v + \frac{p_y}{\rho_b} = 0, \tag{5.2}$$

$$w_t + \overline{U}w_x - f_H\,u + g(-\alpha T_p + \beta S_p) - \nu\nabla^2 w + \frac{p_z}{\rho_b} = 0, \tag{5.3}$$

$$u_x + v_y + w_z = 0, \tag{5.4}$$

$$T_{pt} + \overline{U}T_{px} + vT_{my} + wT_{mz} - \kappa_T\nabla^2 T_p = 0, \tag{5.5}$$

$$S_{pt} + \overline{U}S_{px} + vS_{my} + wS_{mz} - \kappa_S\nabla^2 S_p = 0. \tag{5.6}$$

Next we eliminate u, v and p between (5.1)–(5.4), which yields

$$\mathrm{D}^2\nabla^2 w + f^2 w_{zz} + f_{\mathrm{H}}(f_{\mathrm{H}} + \overline{U}_z)\, w_{yy} + f(\overline{U}_z + 2f_{\mathrm{H}})\, w_{yz} + \frac{g}{\rho_{\mathrm{b}}}\mathrm{D}\nabla_{\mathrm{H}}^2 \rho_{\mathrm{p}} = f_{\mathrm{H}}\, \overline{U}_z (v_x - u_y)_x, \tag{5.7}$$

where the operator D is defined by

$$\mathrm{D} = (\ )_t + \overline{U}(\ )_x - \nu\nabla^2(\ ). \tag{5.8}$$

We will only discuss two cases of a perturbation flow, namely one with velocity parallel to the (y,z)-plane with $\overline{U}_z$ = constant, and another perturbation flow with velocity in the (x,z)-plane and with $\overline{U}$ = constant. This allows us to deal with an equation with constant coefficients. Therefore, because of assumed independence of x in the first case and because $\overline{U}_z = 0$ in the second case, the term on the right-hand side of (5.7) vanishes, and so cross-differentiation, which would raise the equation to higher order to eliminate the term, is unnecessary.

We now consider a perturbation flow in the (y,z)-plane independent of x. Using continuity (5.4), the heat and salt perturbation equations become

$$\mathrm{D}_T T_{\mathrm{p}y} = T_{\mathrm{m}y} w_z - T_{\mathrm{m}z} w_y, \tag{5.9}$$

$$\mathrm{D}_S S_{\mathrm{p}y} = S_{\mathrm{m}y} w_z - S_{\mathrm{m}z} w_y. \tag{5.10}$$

The operators D_T and D_S are defined by

$$\mathrm{D}_T = (\ )_t + \overline{U}(\ )_x - \kappa_T\nabla^2(\ ), \tag{5.11}$$

$$\mathrm{D}_S = (\ )_t + \overline{U}(\ )_x - \kappa_S\nabla^2(\ ), \tag{5.12}$$

After combining (5.7), (5.9) and (5.10), we obtain the single equation for the vertical velocity fluctuations in the (y,z)-plane:

$$\begin{aligned}\mathrm{D}_T\,\mathrm{D}_S\,\mathrm{D}^2\nabla^2 w + f^2\,\mathrm{D}_T\,\mathrm{D}_S\, w_{zz} + f_{\mathrm{H}}(f_{\mathrm{H}} + \overline{U}_z)\,\mathrm{D}_T\,\mathrm{D}_S\, w_{yy} \\ + f(\overline{U}_z + 2f_{\mathrm{H}})\,\mathrm{D}_T\,\mathrm{D}_S w_{yz} + \alpha g(T_{\mathrm{m}z}\,\mathrm{D}\mathrm{D}_S w_{yy} - T_{\mathrm{m}y}\,\mathrm{D}\mathrm{D}_S w_{zy}) \\ + \beta g(-S_{\mathrm{m}z}\,\mathrm{D}\mathrm{D}_T w_{yy} + S_{\mathrm{m}y}\,\mathrm{D}\mathrm{D}_T w_{yz}) = 0.\end{aligned} \tag{5.13}$$

6. Planar-wave solutions

Equation (5.13) is a linear equation with y- and z-dependent coefficients involving gradients of $\overline{U}(z)$, $T_{\mathrm{m}}(y,z)$ and $S_{\mathrm{m}}(y,z)$. For the purpose of demonstrating the sensitivity of thermohaline stability to rotation and shear in a simple manner, we assume constant gradients of T_{m} and S_{m}. Thus the geostrophic shear $\overline{U}_{\mathrm{g}z}$ is also constant. Since we consider waves independent of x and propagating normally to $\overline{U}(z)$ in the (y,z)-plane, the D, D_T and D_S operators will not contain an advective term. Furthermore, we require that the ageostrophic shear $\overline{U}_{\mathrm{a}z}$ = constant, and therefore the total shear $\overline{U}_z$ = constant, so that (5.13) will have constant coefficients.

Letting $T_{\mathrm{m}y}$, $T_{\mathrm{m}z}$, $S_{\mathrm{m}y}$, $S_{\mathrm{m}z}$ and $\overline{U}_z$ be constant, there will be solutions for w of the form

$$w(x,y,z,t) = \mathrm{Re}\, w_1 \exp[\mathrm{i}(ly + mz) + pt]\}. \tag{6.1}$$

Because superposition of solutions is permissible, this form of the solution includes standing and travelling waves in both the y- and z-directions. Here w_1 represents a complex constant, l and m are the y- and z-wavenumbers, and the generally complex quantity p defines frequency and temporal growth rate. Substitution from (6.1) into (5.13), after eliminating the exponential, yields the characteristic equation for the

'(y,z)-wave' ($k=0$), as follows:

$$(p+\nu\kappa^2)\,[-(p+\kappa_T\kappa^2)\,(p+\kappa_S\kappa^2)\,(p+\nu\kappa^2)\,\kappa^2+\alpha gl(mT_{my}-lT_{mz})\,(p+\kappa_S\kappa^2)$$
$$-\beta gl(mS_{my}-lS_{mz})\,(p+\kappa_T\kappa^2)]-(mf+lf_H)\,(mf+lf_H+l\overline{U}_z)\,(p+\kappa_T\kappa^2)\,(p+\kappa_S\kappa^2)=0. \tag{6.2}$$

Here the wavenumber vector $\boldsymbol{\kappa}=(l,m)$, and its magnitude is denoted by κ. Next we introduce the Prandtl number $\sigma=\nu/\kappa_T$, the diffusivity ratio $\tau=\kappa_S/\kappa_T$, and the new dependent variable $q=p/\kappa_T\kappa^2$ used by Baines & Gill (1969), which eliminates an explicit dependence on wavenumber. The characteristic equation can be expressed in terms of q as

$$(q+\sigma)\,[(q+1)\,(q+\tau)\,(q+\sigma)-\sigma\tilde{R}_T(q+\tau)+\sigma\tilde{R}_S(q+1)]+A(q+1)\,(q+\tau)=0. \tag{6.3}$$

The parameter A contains the effects of rotation and mean shear:

$$A=\frac{(mf+lf_H)\,(mf+lf_H+l\overline{U}_z)}{\kappa_T^2\kappa^6}. \tag{6.4}$$

The thermal and solutal Rayleigh numbers are

$$\tilde{R}_T=\frac{\alpha gl(mT_{my}-lT_{mz})}{\kappa_T\nu\kappa^6}, \tag{6.5}$$

$$\tilde{R}_S=\frac{\beta gl(mS_{my}-lS_{mz})}{\kappa_T\nu\kappa^6}. \tag{6.6}$$

Thus the system reduces to the independent variable q as a function of the three parameters A, $\tilde{R}_S$, $\tilde{R}_T$.

To understand the parameters A, $\tilde{R}_S$ and $\tilde{R}_T$, physically, an alternative formulation is presented. Define the direction of the temperature gradient along the unit vector $\hat{\boldsymbol{s}}_T$. Then

$$\frac{dT_m}{ds_T}\hat{\boldsymbol{s}}_T=\boldsymbol{\nabla}T_m=(T_{my},T_{mz})=T_{ms}(\cos\phi_T,\sin\phi_T), \tag{6.7}$$

and similarly for salinity,

$$\frac{dS_m}{ds_S}\hat{\boldsymbol{s}}_S=\boldsymbol{\nabla}S_m=(S_{my},S_{mz})=S_{ms}(\cos\phi_S,\sin\phi_S). \tag{6.8}$$

Let the wavenumber vector be

$$\boldsymbol{\kappa}=(l,m)=\kappa(\cos\theta,\sin\theta) \tag{6.9}$$

and the latitude be λ, so that

$$\boldsymbol{\Omega}=\tfrac{1}{2}(f_H,f)=\Omega(\cos\lambda,\sin\lambda), \tag{6.10}$$

where $\boldsymbol{\Omega}$ is the Earth's rotation. Scaling the velocity with 2Ω, we define

$$\mathscr{U}_z=\frac{\overline{U}_z}{2\Omega}. \tag{6.11}$$

Then

$$\tilde{R}_S=\frac{\beta g}{\nu\kappa_T\kappa^4}S_{ms}\cos\theta\sin(\theta-\phi_S), \tag{6.12}$$

$$\tilde{R}_T=\frac{\alpha g}{\nu\kappa_T\kappa^4}T_{ms}\cos\theta\sin(\theta-\phi_T), \tag{6.13}$$

$$A=\frac{4\Omega^2}{\kappa_T^2\kappa^4}[\cos(\theta-\lambda)+\mathscr{U}_z\cos\theta]\cos(\theta-\lambda). \tag{6.14}$$

From (6.12)–(6.14) the following statements can be made.

(1) The angles between the wavenumber vector and the salinity and temperature gradients determine the size of $\tilde{R}_S$ and $\tilde{R}_T$ respectively.

(2) If the wave is travelling up or down the temperature or salinity gradient, then $\tilde{R}_T$ or $\tilde{R}_S$ is zero respectively.

(3) Waves travelling perpendicular to the temperature or salinity gradients have the highest $\tilde{R}_T$ or $\tilde{R}_S$ magnitudes respectively. In an oceanographic geostrophic flow, such waves are usually horizontally travelling waves since $T_{my} \ll T_{mz}$ and $S_{my} \ll S_{mz}$.

(4) The Rayleigh numbers are positive for $\theta - \phi_S > 0$ or $\theta - \phi_T > 0$ and conversely. Thus if $\phi_S \approx \phi_T \approx 90°$ (approximately vertical stratification), Rayleigh numbers are negative only for waves having both northward and upward components.

(5) The factor $\cos(\theta - \lambda)$ in A is maximum when the wavenumber vector is aligned with the rotation vector $\boldsymbol{\Omega}$, and minimum when the wavenumber vector and rotation vector are in opposite directions, while A is zero when they are perpendicular. Thus the product of the planetary vorticity component and the total mean-field vorticity component in the direction of the wavenumber vector determine A.

(6) On the equator ($\lambda = 0$), the sign of A is determined by $\mathscr{U}_z$. For $\mathscr{U}_z < -1$, $A < 0$, and conversely. This corresponds to a shear of $\overline{U}_z < -1.45 \times 10^{-4}$, a region of negative shear such as above an eastward jet or below a westward jet.

(7) Since $\phi_S \approx \phi_T \approx 90°$ in the ocean, $\rho_{ms} \approx \rho_{mz} = 0$ for $\tilde{R}_T = \tilde{R}_S$, so that, in the parameter space $(A, \tilde{R}_S, \tilde{R}_T)$, the plane $\tilde{R}_S = \tilde{R}_T$ can be identified as the plane of neutral gravitational stability.

7. The stability diagram

The introduction of rotation and shear, as shown by (6.3), represents a singular perturbation of the non-rotating case. Setting the quantity in the square brackets equal to zero gives the characteristic equation obtained by Baines & Gill (1969) for zero rotation and shear. Our definitions of $\tilde{R}_S$ and $\tilde{R}_T$ are more general because they include the horizontal density gradient which satisfies the thermal wind balance (4.7). When A differs from zero, the additional factor $q + \sigma$ multiplies the square bracket, and there is a term containing A. The polynomial for q is thus increased by one degree, and a new root is introduced. It is also interesting to note from the form of the expression for A in (6.4) that, in the absence of rotation, constant shear has no effect, while in the absence of shear, rotation still has an effect. Equation (6.4) shows that a change in sign of $\overline{U}_z$ changes the magnitude of A, so both the sign and the magnitude are important.

For the special case $A = 0$, the results of Baines & Gill (1969) were obtained and have been recalculated to show certain intercepts of stability boundaries. The results are shown in figure 1. The line $\tilde{R}_T = \tilde{R}_S$, which we identify as $\mathrm{d}\rho/\mathrm{d}z = 0$, as mentioned in §6, is the locus of neutrally stable density stratification. The region to the right and below that line represents a gravitationally stable domain, where internal waves are possible. The area in the third quadrant between the line $\mathrm{d}\rho/\mathrm{d}z = 0$ and the stability boundary XZ, which is near the negative $\tilde{R}_T$ axis, is the regime where salt fingering occurs. Here a stable density stratification formed by warm salt water overlying colder fresher water is convectively unstable. The region where viscous and diffusive effects inhibit overstable oscillations is to be found near the origin in the first quadrant. The line XW represents the neutral-stability boundary for overstable oscillations. Near the $\tilde{R}_T$ axis, this region extends only to unstable density stratifications, but the stability boundary crosses the line $\mathrm{d}\rho/\mathrm{d}z = 0$ at a value of

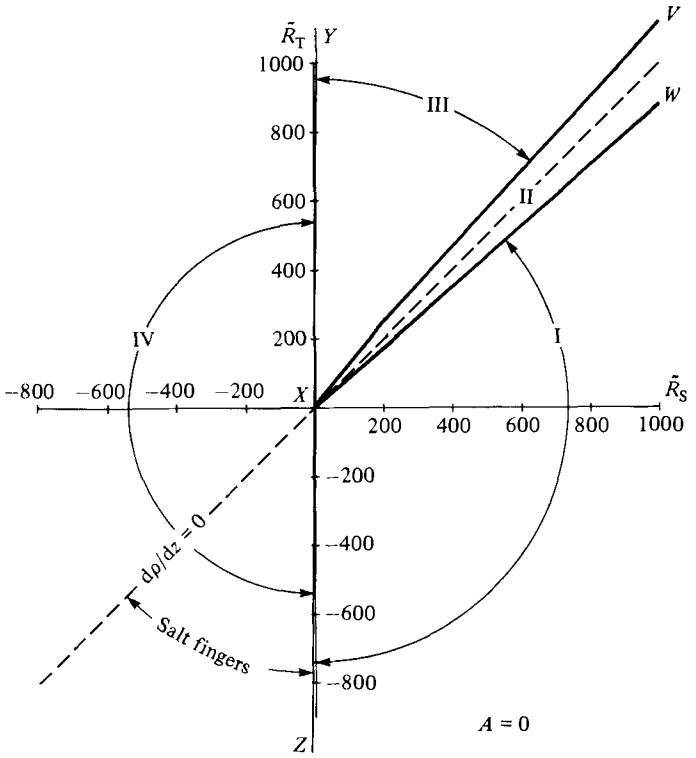

FIGURE 1. Stability diagram, showing regions in the $(\tilde{R}_S, \tilde{R}_T)$-plane for $A = 0$. Region I: all roots stable ($q_r < 0$). Region II: overstable oscillations (2 complex roots, $q_r > 0$, 2 real roots, $q_r < 0$). Region III: 2 divergent modes (4 real roots, $q_r > 0$ for two roots). Region IV: one divergent mode (four real roots, $q_r > 0$ for one root). The neutral gravitational stability boundary is $d\rho/dz = 0$, with the stable regime to the right.

$\tilde{R}_T = \tilde{R}_S = 8.17$ ($\tau \approx 0.01, \sigma = 7$ for sea water). For larger values of $\tilde{R}_S$, the overstable oscillations can occur also for gravitationally stable density gradients. In this range, internal waves will gain buoyancy near their crests and lose buoyancy near the troughs, and become amplified. The changes in buoyancy are due mostly to heat diffusion, the diffusivity of salt being so much smaller. The other boundary for the overstable domain, XV, is to be found in the gravitationally unstable regime. At this boundary, purely exponentially divergent tumbling of the unstable density field takes over.

We consider next how a mean shear will change the stability. McIntyre (1970*a*, *b*) examined the combined effect of diffusion of heat and momentum in a rotating system and found that instability is possible, as was confirmed by Calman (1977) in a series of experiments. Our results represent an extension of their findings to triple-diffusive systems where heat, salt and momentum diffusion all occur, and include their results. According to (6.4), mean shear, in the absence of rotation, has no direct effect. One effect of a mean shear is the kinematic distortion of initial three-dimensional disturbances, as discussed by Landahl (1980). We shall disregard this effect and concentrate on the simpler direct effects of shear upon stability, as expressed in (6.3) and shown in figures 2–6. For A different from zero, we used the same technique as Baines & Gill (1969) and Veronis (1965) to find the lines corresponding to the stability boundaries ZXY and XW. There is now a quadratic expression for the

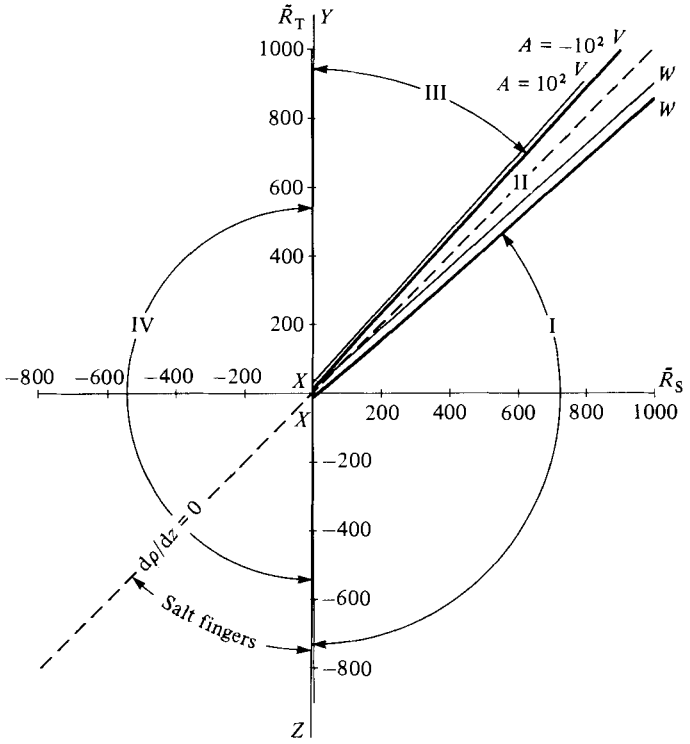

FIGURE 2. Stability diagram for $A = 10^2$ and $A = -10^2$. The regions are labelled as in figure 1. Note change in boundaries for region II.

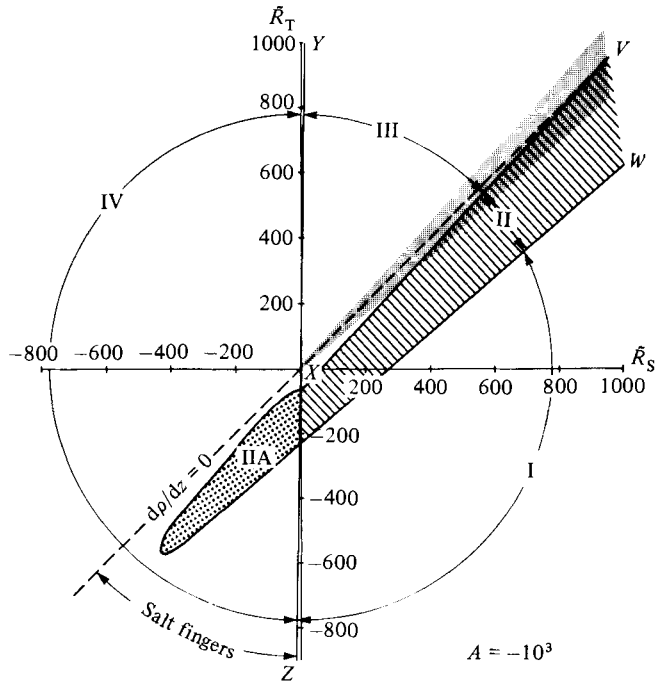

FIGURE 3. Stability diagram for $A = -10^3$. Regions labelled as in figure 1, with the additional region IIA, having one divergent mode ($q_r > 0$, $q_i = 0$) and two overstable modes ($q_r > 0$, $q_i \neq 0$). Region IIA is entirely in the third quadrant, to the left of the line XZ.

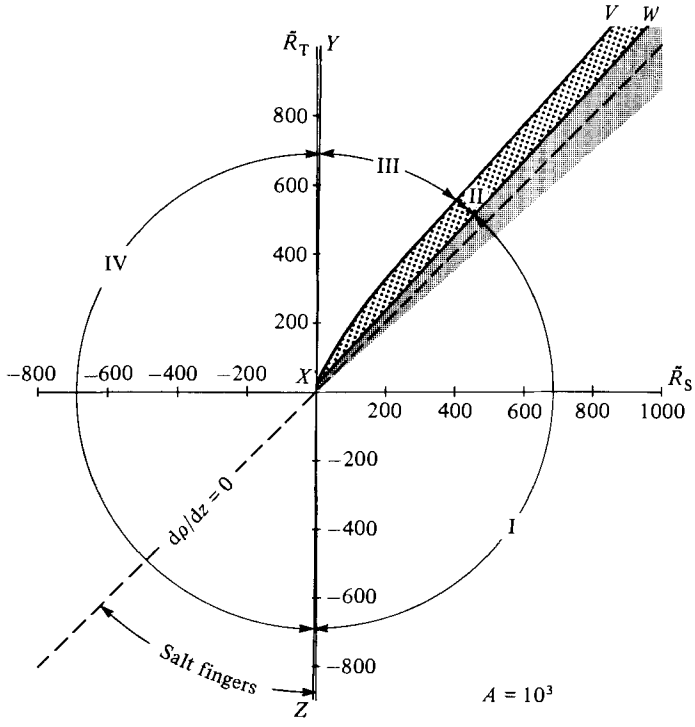

FIGURE 4. Stability diagram for $A = 10^3$. Regions labelled as in figure 1.

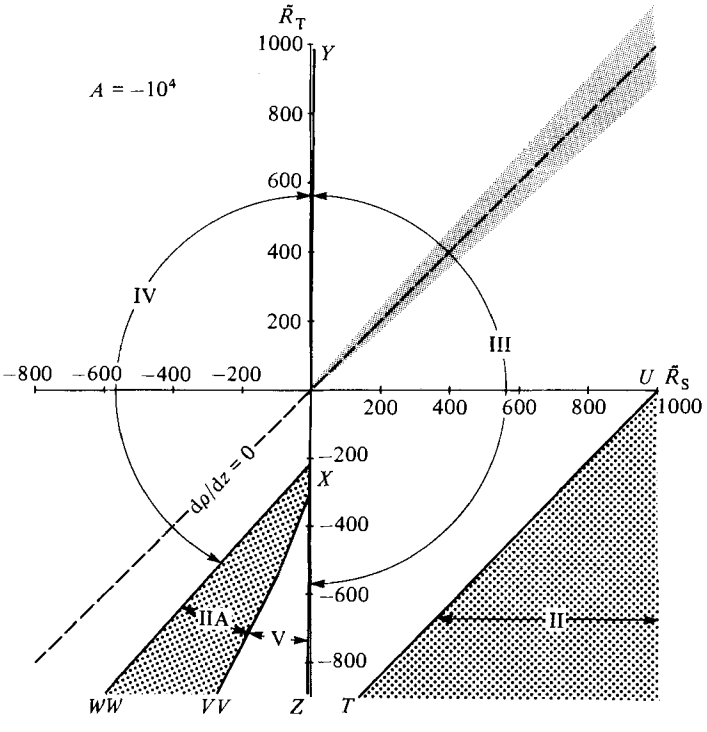

FIGURE 5. Stability diagram for $A = -10^4$. Regions labelled as in figure 3 with the additional region V, having three divergent modes ($q_r > 0$, $q_i = 0$). The region IIA is bounded by X–WW and X–VV.

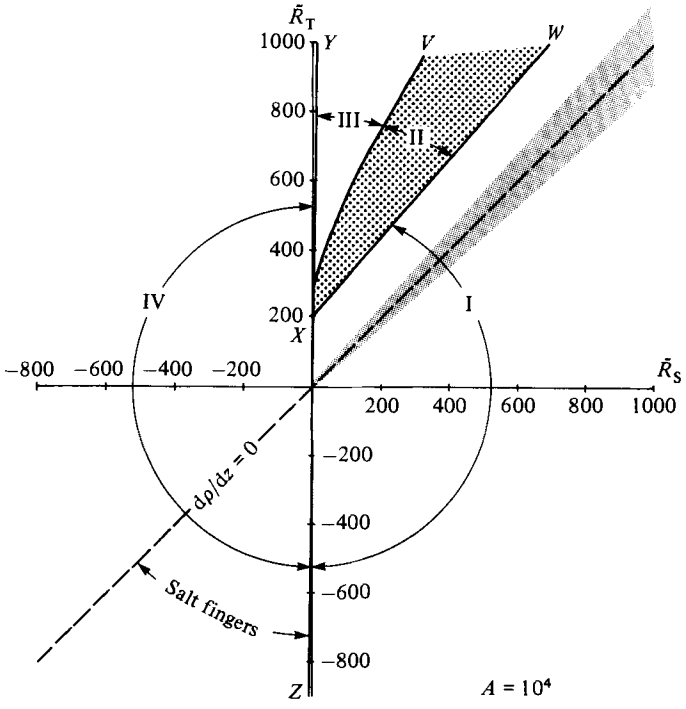

FIGURE 6. Stability diagram for $A = 10^4$. Regions labelled as in figure 1.

boundary XW. The stability boundary corresponding to XV in the case $A = 0$ is awkward to find for $A \neq 0$ using standard analytical techiques (cf. Abramowitz & Stegun 1965), so we found iteration methods more convenient. We therefore mapped out, on a set of grid points in the $(\tilde{R}_S, \tilde{R}_T)$-plane, the types of roots of (6.3). Then, when a change in type of roots was found between two adjacent grid points, we solved by iteration to locate the stability boundary where the root changed character.

Figures 2–6 show the stability diagrams for $A = \pm 10^2$, -10^3, 10^3, -10^4 and 10^4 respectively. In these figures, as in figure 1, the region of overstable oscillations, II, is where (6.3) has two complex roots with positive real parts. This region shifts further into the stably stratified region of the $(\tilde{R}_S, \tilde{R}_T)$-plane as A decreases from 0 to -10^2 (figure 2) and further to -10^3 (figure 3). For comparison, region II for $A = 0$ is indicated in the diagrams in figures 3–6 by light shading. Positive values of A shift the overstable region further into the negative $\mathrm{d}\rho/\mathrm{d}z$ region, as can be seen in figures 2, 4 and 6.

For all values of A shown in figures 2–6, there is a direct instability mode, corresponding to salt-finger instability, in the third quadrant between the line XZ and $\mathrm{d}\rho/\mathrm{d}z = 0$. For $A = -10^3$, however, the overstable oscillation regime has invaded the salt-finger regime, indicated in figure 3 as region II A, to the left of XZ. Here there is still one direct mode ($q_r > 0$, $q_i = 0$), corresponding to salt-finger instability and two overstable modes ($q_r > 0$, $q_i \neq 0$). For $A = 10^3$, the overstable oscillatory instability domain moves further into the gravitationally unstable domain, remaining entirely in the first quadrant of the diagram, as shown in figure 4 and, for $A = 10^4$, in figure 6. For a still more negative value, namely $A = -10^4$, the overstable region II moves far into the fourth and third quadrants, as shown in figure 5. Region II A still contains a direct mode, corresponding to what may be called a longitudinal roll

vortex pattern (see Hsu 1974), and two overstable oscillatory modes. Note that region II in figure 5 looks like a magnified picture of the region near the origin of figure 3, and is consistent with a continuous change from figure 3 to 5. The loss of contact between regions II and II A as occurs in figure 5 and the appearance of region V, where there are three direct modes, are new features. An instability for which the growth rate depends solely upon the mean vertical density gradient $\mathrm{d}\rho/\mathrm{d}z$ is the well-known baroclinic instability, modified by diffusive effects, rather than an instability driven by diffusion. In figure 3 the stability boundaries for regions II and II A are not parallel to the $\mathrm{d}\rho/\mathrm{d}z = 0$ line, so we can conclude that diffusive or double-diffusive effects are significant. A stability boundary parallel to $\mathrm{d}\rho/\mathrm{d}z = 0$ indicates that the density stratification is the important variable. If the boundary is inclined to $\mathrm{d}\rho/\mathrm{d}z =$ constant lines, salinity and temperature affect the stability in a manner that cannot be explained solely in terms of their contributions to density. In figure 5 the boundary of region II is nearly parallel to the $\mathrm{d}\rho/\mathrm{d}z = 0$ line and is most likely a baroclinic instability somewhat modified by diffusion and also affected by the inclusion of the horizontal component of rotation f_{H}. We have not assessed the relative importance of the diffusive, rotary, stratification and shear effects for the overstable oscillations. In all cases at least one direct unstable mode occurs in the gravitationally unstable regime and above the XV boundary. Since all the modes are periodic in y, normal to the mean velocity $\bar{U}$, we may think of the direct modes as longitudinal modes or the initial instability that can lead to streamwise roll vortices. The instability found by McIntyre (1970*a*, *b*) occurs at $\tilde{R}_S = 0$ on the $\tilde{R}_T$ axis and corresponds to regions II and II A where they intersect the $\tilde{R}_T$ axis in the $(\tilde{R}_S, \tilde{R}_T)$-plane. A better representation of the McIntyre instability would be a plot of the stability boundary in the $(A, \tilde{R}_T)$-plane for $\tilde{R}_S = 0$.

Because shear is involved, the Richardson number for the flow is of interest. The Richardson-number criterion for the instability of two-dimensional stratified flow does not strictly apply here, since the modes propagate normally to the mean flow. But the same idea of resonance between the Brunt–Väïsälä frequency $N = -[(g/\rho)\,\mathrm{d}\rho/\mathrm{d}z]^{\frac{1}{2}}$ and the angular velocity ω of particles in the mean flow, $\omega = 2\bar{U}_z$, may still be used as a possible criterion for neutral stability. Thus the frequency ratio $N^2/\omega^2 = 1$ for resonance gives a critical Richardson number of $Ri_{\mathrm{cr}} = N^2/4\bar{U}_z^2 = \frac{1}{4}$. Writing the Richardson number in terms of $\tilde{R}_S$, $\tilde{R}_T$ and A results in

$$\mathrm{Ri} = \frac{[\sigma(\tilde{R}_S - \tilde{R}_T) - \tilde{U}_{gz} E^{-1}]\,(E^{-1} + E_{\mathrm{H}}^{-1})^2}{[A - (E^{-1} + E_{\mathrm{H}}^{-1})^2]^2}, \tag{7.1}$$

where we have defined the Ekman numbers E and E_{H} as

$$E = \frac{\kappa_T \kappa^3}{mf}, \tag{7.2}$$

$$E_{\mathrm{H}} = \frac{\kappa_T \kappa^3}{lf_{\mathrm{H}}}, \tag{7.3}$$

and the non-dimensionalized geostrophic velocity as

$$\tilde{U}_{gz} = \frac{l\bar{U}_{gz}}{\kappa_T \kappa^3}. \tag{7.4}$$

Thus small Richardson numbers are possible for large values of A, allowing for resonance and possibly associated instability to intrude far into the fourth quadrant of the $(\tilde{R}_S, \tilde{R}_T)$-plane.

The question may arise: does the direct, salt-finger mode grow faster or slower than the overstable oscillation in region II A in figures 3 and 5? These two modes need not compete with each other since the overstable oscillations may be thought of as travelling waves which grow as they move, while the direct mode grows in one place. To satisfy our curiosity about relative growth rates, we cite as an example the case $(\tilde{R}_S, \tilde{R}_T, A) = (-100, -200, -1000)$. In the region II A, the roots are $(q_r, q_i) = (1.65, 0)$, $(-27.9, 0)$, $(5.62, 8.52)$ and $(5.62, -8.52)$. Thus the growth rate of the overstable mode ($q_i \neq 0$) is clearly larger than that of the direct mode. For this particular set of Rayleigh numbers, the overstable mode has the largest growth rate at $A \approx 1200$.

The effects of rotation and shear on the stability boundaries for salt-fingering instability are small, in comparison with the effects on overstable oscillations, as has been discussed by Schmitt & Lambert (1979). The boundary for the salt-finger instability, the line ZX in figures 2–6, changes only its intercept $1.0 + A/\sigma^2$ with the $\tilde{R}_T$ axis and not the slope τ^{-1} with changing A, although an overstable, oscillatory instability invades the third quadrant. Then two more direct modes appear as A decreases.

In order to illustrate further how the roots change as a function of the parameter A, figures 7 and 8 show two cases. Figure 7 shows the change in roots at the point $(\tilde{R}_S, \tilde{R}_T) = (100, 88.636)$, a point on the XW neutral stability boundary of the Baines & Gill (1969) stability diagram (figure 1). For $A = 0$, the real parts of all roots are zero or negative, while two roots, corresponding to internal waves, have imaginary parts. As A becomes negative, the real parts of the oscillatory roots corresponding to internal waves become large and positive, while the real roots corresponding to exponential growth or decay are negative. For smaller values of A than $A = -500$, the growth rate of one complex root becomes extremely large while the other decreases to a small value and the frequency goes to zero, causing the overstable modes to become direct modes. Figure 8 shows the change in the roots q as a function of A for the point $(\tilde{R}_S, \tilde{R}_T) = (-100, -400)$, which lies in the salt-finger regime for $A = 0$ (see figure 1). At a value of $A \approx -1400$, the oscillatory modes attain positive growth rates larger than the salt-finger mode (curve 4). Then at $A \approx -3400$, the frequencies go to zero, with one of the oscillatory modes becoming a fast-growing direct mode and the other a slower-growing direct mode. Between $A \approx -3400$ and -5800, there are three direct modes. The slow-growing direct modes become overstable modes for A between -5800 and -43000. For $A < -43000$ there are two stable modes. Note that the curve 4 has $q_r > 0$, but, on the scale used in figure 8, it appears just above the A-axis.

Although Stern (1975) found that (y, z)-waves grow faster than (x, z)-waves for a layer bounded by flat walls, it is possible that an (x, z)-wave may grow faster than a (y, z)-wave in the present case. The (x, z)-wave solution will have an analogous form to (6.1) for the case of constant mean-field velocity $\bar{U}$ = constant. For this case A becomes E^{-2}, and thus $A \geqslant 0$. For the (y, z)-wave with $\bar{U}$ = constant, $A = (E^{-1} + E_H^{-1})^2$, and E and E_H can have opposite signs depending on the wave-number vector. Thus the (x, z)-wave behaviour does not seem substantially different from that of the (y, z)-wave. The attraction of the analysis for a transverse wave is its simplicity, while maintaining the essential character of the solution. The essential result, that unstable waves can exist in the third and fourth quadrants of the stability diagram in the presence of rotation and shear, is not expected to change.

The oceanic application of the result that double-diffusive effects in the presence of rotation and shear can produce growing waves depends on the fact that a density

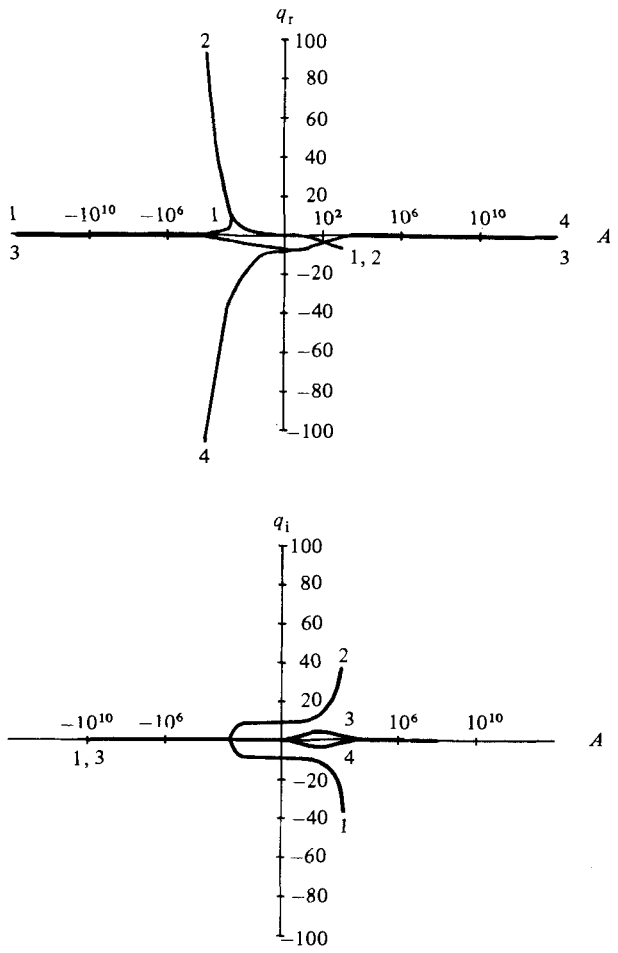

FIGURE 7. Dependence of (*a*) real and (*b*) imaginary parts of roots $q = q_r + iq_i$ of characteristic equation (6.3) on the parameter A for the point $\bar{R}_S = 100.0$, $\bar{R}_T = 88.636$ in the stability diagram, which is on the stability boundary XW in figure 1.

stratification in a flow without mean shear tends to suppress turbulence; so that, on the average in the ocean, the turbulence level is very small as measured, for example, in terms of a velocity scale based on stability and wavenumber, $[-g(\mathrm{d}\rho/\mathrm{d}z)/\rho]^{\frac{1}{2}}/\kappa = N/\kappa$.

8. Variable shear and variable stratification

Allowing the shear $\overline{U}_z$ and the temperature and salinity stratification to vary, and carrying out the linear perturbation analysis but neglecting fourth and higher derivatives of $\overline{U}(z)$, we obtain for a perturbation in the (y, z)-plane

$$[\mathrm{D}_S\,\mathrm{D}_T\,\mathrm{D}^2\nabla^2 w + f^2\mathrm{D}_S\,\mathrm{D}_T\,w_{zz} + f_{\mathrm{H}}(f_{\mathrm{H}} + \overline{U}_z)\,\mathrm{D}_S\,\mathrm{D}_T\,w_{yy} + f(\overline{U}_z + 2f_{\mathrm{H}})\,\mathrm{D}_S\,\mathrm{D}_T\,w_{yz}$$
$$- g\alpha\mathrm{D}_S\,\mathrm{D}(w_{yz}\,T_{\mathrm{m}y} - w_{yy}\,T_{\mathrm{m}z}) + g\beta\mathrm{D}_T\,\mathrm{D}(w_{yz}\,S_{\mathrm{m}y} - w_{yy}\,S_{\mathrm{m}z})] + \overline{U}_{zz} f\,\mathrm{D}_S\,\mathrm{D}_T\,w_y = 0. \tag{8.1}$$

This equation shows that $\overline{U}_{zzz}$ has no effect on stability, while the effects of $\overline{U}_{zzzz}$ and higher derivatives exist and have been neglected. The coefficients in (8.1) depend upon

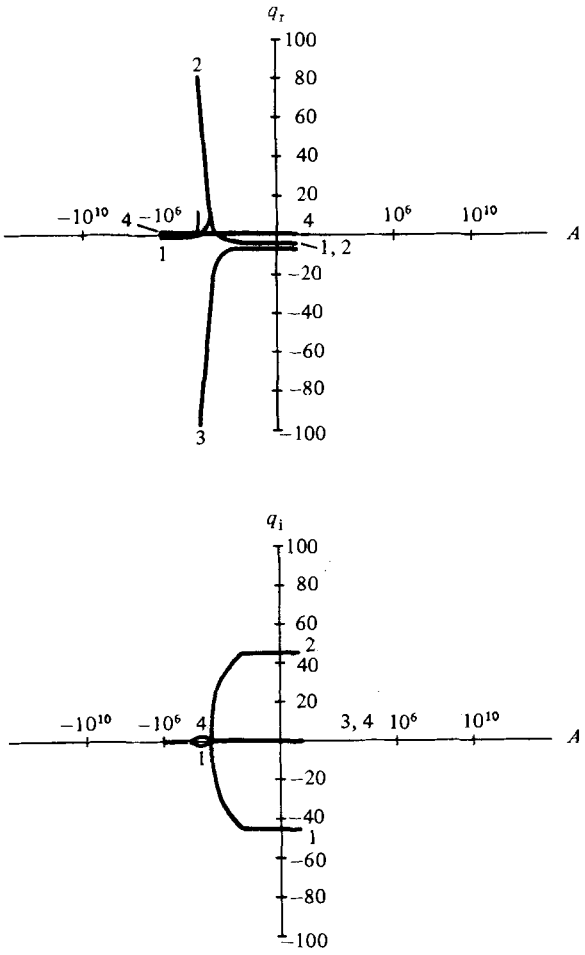

FIGURE 8. Same as in figure 7, but for the point $\bar{R}_S = -100.0$, $\bar{R}_T = -400.0$, which is in region IV in the salt-finger regime in figure 1. Note the occurrence of oscillatory instability for certain values of A negative.

z through the presence of derivatives of $\overline{U}(z)$ and on y and z through T_{my}, T_{mz}, S_{my} and S_{my} terms. For the special case of $\mathrm{d}w/\mathrm{d}x = 0$ considered here, there is only one $\overline{U}_{zz}$ term. The coefficient of $\overline{U}_{zz}$ is $f\,\mathrm{D}_S\,\mathrm{D}_T\,w_y$, showing that, for this case, the effect of $\overline{U}_{zz}$ includes rotation. For this particular case it may be possible to develop necessary criteria for stability by using an extension of Synge's (1938) method, and one may even be able to find full solutions for special choices of stratification. We leave this to others, and conclude by remarking that the effect of variable velocity shear is also influenced by rotation. In the more general case, we expect that $\overline{U}_{zz}$ will have an effect even for zero rotation, as was pointed out by Rayleigh (1878) for neutral stratification.

9. Fluxes

The solution for simple harmonic dependence on y, z, t can be combined to represent horizontally travelling waves with harmonic z-dependence as well as planar waves. But the fluxes of momentum, salt, heat and mass induced by different superpositions

of planar waves will be different. Flux calculations for planar waves and horizontally propagating waves are presented in this section. These fluxes are induced by the presence of the internal waves serving as an external modulator of the flow field and are not the fluxes carried by the wave field.

Wave growth is not needed to induce fluxes which may lead to layer formation. Waves that propagate through a region will also induce mean fluxes. We suggest that these wave-induced fluxes may well prove to be geophysically important.

9.1. *Obliquely propagating waves*

First consider a planar wave propagating in a direction tilted with respect to the horizontal, where the vertical velocity field w is given by

$$w(y,z,t) = \hat{w}\cos(ly+mz+p_{\mathrm{i}}t)\exp(p_{\mathrm{r}}t). \tag{9.1}$$

Since $u_x = 0$, v is found from continuity (5.4), from which we obtain after integration in y

$$v = -\frac{m}{l}\hat{w}\exp(p_{\mathrm{r}}t)\cos\phi. \tag{9.2}$$

Here $\phi = ly+mz+p_{\mathrm{i}}t$. Using the x-momentum equation (5.1) and (9.2), we find that u can be written as

$$u = \exp(p_{\mathrm{r}}t)(u_{\mathrm{a}}\cos\phi + u_{\mathrm{b}}\sin\phi), \tag{9.3}$$

where

$$u_{\mathrm{a}} = -\hat{w}\left[\bar{U}_z + f_{\mathrm{H}} + \frac{m}{l}f\right](p_{\mathrm{r}}+\nu\kappa^2)[(p_{\mathrm{r}}+\nu\kappa^2)^2+p_{\mathrm{i}}^2]^{-1}, \tag{9.4}$$

$$u_{\mathrm{b}} = -\hat{w}p_{\mathrm{i}}\left[\bar{U}_z + f_{\mathrm{H}} + \frac{m}{l}f\right][(p_{\mathrm{r}}+\nu\kappa^2)^2+p_{\mathrm{i}}^2]^{-1}. \tag{9.5}$$

Using (9.1)–(9.3) and approximating the momentum flux by averaging over the phase ϕ, we find the wave-induced fluxes of eastward (x) and northward (y) momentum

$$\langle uw\rangle = \frac{-\hat{w}^2[\bar{U}_z + f_{\mathrm{H}} + (m/l)f](p_{\mathrm{r}}+\nu\kappa^2)\exp(2p_{\mathrm{r}}t)}{2[(p_{\mathrm{r}}+\nu\kappa^2)^2+p_{\mathrm{i}}^2]}, \tag{9.6}$$

$$\langle vw\rangle = -\frac{m}{2l}\hat{w}^2\exp(2p_{\mathrm{r}}t). \tag{9.7}$$

The phase average is denoted by $\langle\ \rangle$. This approximation is valid when $p_{\mathrm{r}} \ll p_{\mathrm{i}}$. The eastward flux of northward momentum is proportional to the vertical flux of eastward momentum:

$$\langle uv\rangle = -\frac{m}{l}\langle uw\rangle. \tag{9.8}$$

The temperature field is calculated by substituting for v and w in the heat-transport equation (5.5)

$$T_{\mathrm{p}} = \frac{\hat{w}[(m/l)T_{my} - T_{mz}]\exp(p_{\mathrm{r}}t)[(p_{\mathrm{r}}+\kappa_T\kappa^2)\cos\phi + p_{\mathrm{i}}\sin\phi]}{(p_{\mathrm{r}}+\kappa_T\kappa^2)^2+p_{\mathrm{i}}^2}, \tag{9.9}$$

resulting in the wave-induced vertical heat flux, using the phase-average approximation,

$$\langle wT_{\mathrm{p}}\rangle = \frac{\hat{w}^2\left[\frac{m}{l}T_{my} - T_{mz}\right](p_{\mathrm{r}}+\kappa_T\kappa^2)\exp(2p_{\mathrm{r}}t)}{2[(p_{\mathrm{r}}+\kappa_T\kappa^2)^2+p_{\mathrm{i}}^2]}. \tag{9.10}$$

The wave-induced salt flux is found by the same methods to be

$$\langle wS_{\mathrm{p}}\rangle = \frac{\hat{w}^2[(m/l)S_{my} - S_{mz}]\exp(2p_{\mathrm{r}}t)(p_{\mathrm{r}}+\kappa_S\kappa^2)}{2[(p_{\mathrm{r}}+\kappa_S\kappa^2)^2+p_{\mathrm{i}}^2]}. \tag{9.11}$$

The wave-induced horizontal fluxes of heat are

$$\langle uT_\mathrm{p}\rangle = \frac{-\hat{w}^2[(m/l)\,T_{\mathrm{m}y}-T_{\mathrm{m}z}]\,[\overline{U}_z+f_\mathrm{H}+(m/l)f]\,[(p_\mathrm{r}+\nu\kappa^2)\,(p_\mathrm{r}+\kappa_T\,\kappa^2)^2+p_\mathrm{i}^2]\exp(2p_\mathrm{r}t)}{2[(p_\mathrm{r}+\nu\kappa^2)^2+p_\mathrm{i}^2]\,[(p_\mathrm{r}+\kappa_T\,\kappa^2)^2+p_\mathrm{i}^2]}, \tag{9.12}$$

$$\langle vT_\mathrm{p}\rangle = -\frac{m}{l}\langle wT_\mathrm{p}\rangle. \tag{9.13}$$

Analogous expressions can be derived for $\langle uS_\mathrm{p}\rangle$ and $\langle vS_\mathrm{p}\rangle$. From the equation of state (3.4), relating ρ', T_p and S_p, we obtain the wave-induced mass flux

$$\langle w\rho'\rangle = (-\alpha\langle wT_\mathrm{p}\rangle+\beta\langle wS_\mathrm{p}\rangle)\,\rho_\mathrm{m}. \tag{9.14}$$

Note that the momentum flux is non-zero, and that the vertical heat and salt fluxes are towards lower temperature and salinity (recall the definitions of the T- and S-fields, (2.1) and (2.2)), while the mass flux can change with the signs of $T_{\mathrm{m}z}$ and/or $S_{\mathrm{m}z}$, depending on their magnitudes. The wave-induced mass flux is negative (downwards) in the second quadrant of the $(\tilde{R}_S, \tilde{R}_T)$-plane and positive (upwards) in the fourth quadrant. The line $\tilde{R}_T = \tilde{R}_S$ forms only an approximate boundary between upward and downward mass flux because of the unequal heat and salt diffusivities κ_T and κ_S, as can be seen by substituting (9.10) and (9.11) into (9.14).

9.2. *Horizontally propagating waves*

For a horizontally propagating modal disturbance we assume

$$w(y,z,t) = \hat{w}\exp(p_\mathrm{r}t)\cos mz\cos\phi, \tag{9.15}$$

where now $\phi = (ly+p_\mathrm{i}t)$. From continuity we find for v the expression

$$v = \frac{m}{l}\hat{w}\exp(p_\mathrm{r}t)\sin mz\sin\phi. \tag{9.16}$$

Finding u from the horizontal momentum equation, we obtain

$$u = \exp(p_\mathrm{r}t)\,[(u_1\cos\phi+u_2\sin\phi)\cos mz+(u_3\cos\phi+u_4\sin\phi)\sin mz], \tag{9.17}$$

where

$$u_1 = -\frac{\hat{w}(p_\mathrm{r}+\nu\kappa^2)}{(p_\mathrm{r}+\nu\kappa^2)^2+p_\mathrm{i}^2},$$

$$u_2 = -\frac{\hat{w}(\overline{U}_z+f_\mathrm{H})\,p_\mathrm{i}}{(p_\mathrm{r}+\nu\kappa^2)^2+p_\mathrm{i}^2},$$

$$u_3 = -\frac{(m/l)\,\hat{w}fp_i}{(p_\mathrm{r}+\nu\kappa^2)^2+p_\mathrm{i}^2},$$

$$u_4 = \frac{(m/l)\,\hat{w}f(p_\mathrm{r}+\nu\kappa^2)}{(p_\mathrm{r}+\nu\kappa^2)^2+p_\mathrm{i}^2}.$$

The vertical fluxes of wave-induced eastward and northward momentum, as estimated by a phase average over ϕ, are

$$\langle uw\rangle = -\frac{\hat{w}^2\exp(2p_\mathrm{r}t)}{4[(p_\mathrm{r}+\nu\kappa^2)^2+p_\mathrm{i}^2]}\left[(p_\mathrm{r}+\nu\kappa^2)\,(1+\cos 2mz)+\frac{m}{l}fp_\mathrm{i}\sin 2mz\right], \tag{9.18}$$

$$\langle vw\rangle = 0. \tag{9.19}$$

The eastward flux of northward momentum is

$$\langle uv\rangle = \frac{m\hat{w}^2 \exp(2p_r t)}{4l[(p_r+\nu\kappa^2)^2+p_i^2]}\left[\frac{m}{l}f(p_r+\nu\kappa^2)(1-\cos 2mz)-p_i(\overline{U}_z+f_H)\sin 2mz\right]. \quad (9.20)$$

There is no vertical flux of northward momentum according to (9.19). Both the vertical flux of eastward momentum (9.18) and the eastward flux of northward momentum (9.20) contain a mean-flux component and an oscillatory component in z with twice the mode-number of the wave. This vertical periodicity in the fluxes allows alternate localized regions of convergence and divergence, resulting in a tendency for momentum layer formation. In order to find the corresponding temperature field let

$$T_p = \exp(p_r t)[(T_1\cos\phi + T_2\sin\phi)\cos mz + (T_3\cos\phi + T_4\sin\phi)\sin mz]. \quad (9.21)$$

Substituting into the heat-flux equation (5.5), setting each relation for the coefficients to zero and solving the resulting equations in $T_1, \ldots, T_4$ yields

$$\begin{pmatrix} T_1 \\ T_2 \\ T_3 \\ T_4 \end{pmatrix} = \frac{\hat{w}}{(p_r+\kappa_T\kappa^2)^2+p_i^2}\begin{pmatrix} -T_{mz}(p_r+\kappa_T\kappa^2) \\ -T_{mz}p_i \\ \frac{m}{l}T_{my}p_i \\ -\frac{m}{l}T_{my}(p_r+\kappa_T\kappa^2) \end{pmatrix}. \quad (9.22)$$

Analogously, for the salinity perturbation we obtain

$$\begin{pmatrix} S_1 \\ S_2 \\ S_3 \\ S_4 \end{pmatrix} = \frac{\hat{w}}{(p_r+\kappa_S\kappa^2)^2+p_i^2}\begin{pmatrix} -S_{mz}(p_r+\kappa_S\kappa^2) \\ -S_{mz}p_i \\ \frac{m}{l}S_{my}p_i \\ -\frac{m}{l}S_{my}(p_r+\kappa_S\kappa^2) \end{pmatrix}. \quad (9.23)$$

The vertical fluxes of heat and salt, found by phase averaging, become

$$\langle wT_p\rangle = \frac{\hat{w}^2\exp(2p_r t)[-T_{mz}(p_r+\kappa_T\kappa^2)(1+\cos 2mz)+(m/l)T_{my}p_i\sin 2mz]}{4[(p_r+\kappa_T\kappa^2)^2+p_i^2)}, \quad (9.24)$$

$$\langle wS_p\rangle = \frac{\hat{w}^2\exp(2p_r t)[-S_{mz}(p_r+\kappa_S\kappa^2)(1+\cos 2mz)+(m/l)S_{my}p_i\sin 2mz]}{4[(p_r+\kappa_S\kappa^2)^2+p_i^2]}. \quad (9.25)$$

The zonal and meridional heat fluxes are given by the expressions

$$\begin{aligned}\langle uT_p\rangle = {} & \tfrac{1}{4}\exp(2p_r t)[(u_1T_1+u_2T_2+u_3T_3+u_4T_4) \\ & +(u_1T_1+u_2T_2-u_3T_3-u_4T_4)\cos 2mz+(u_1T_3+u_3T_1+u_2T_4+u_4T_2)\sin 2mz], \end{aligned} \quad (9.26)$$

$$\langle vT_p\rangle = \frac{m}{4l}\hat{w}\exp(2p_r t)[T_2\sin 2mz + T_4(1-\cos 2mz)], \quad (9.27)$$

where $u_1, \ldots, u_4$ are defined in (9.17), $T_1, \ldots, T_4$ in (9.22), and v in (9.16). For the salt flux, we find an analogous result. The zonal and meridional heat fluxes are composed of both a constant term and an oscillatory term periodic in z.

The vertical gradients of the fluxes are of special interest, since the mean heat flux

equation, with the second-order flux added, takes the form

$$T_{mt}+\kappa_T \nabla^2 T_m = -\frac{\partial \langle wT_p \rangle}{\partial z}. \tag{9.28}$$

The flux term therefore will reveal whether the fluxes tend to smooth out or enhance a temperature gradient. Taking the derivative of (9.24) gives

$$\frac{\partial}{\partial z}\langle wT_p \rangle = \frac{m\hat{w}^2 \exp(2p_r t)\,[T_{mz}(p_r+\kappa_T\kappa^2)\sin 2mz + (m/l)\,T_{my}\,p_i \cos 2mz]}{2[(p_r+\kappa_T\kappa^2)^2+p_i^2]}. \tag{9.29}$$

The flux gradient is periodic in z, and (9.28) shows that there is a tendency for layer formation. In the originally constant gradient, the mean heat flux is toward the layers at $z = n\pi/m$, where n is an integer if the second term in (9.29) is negligible. The mass flux will then be periodic also according to (9.14). The same holds for the salinity. The tendency for layer formation in a thermohaline convective system was first suggested by Turner & Stommel (1964). Our analysis adds a more quantitative explanation and shows how the tendency for layering depends on the vertical wavenumber, which, in turn, may well be influenced by the larger-scale vertical fine-structure field.

Comparison between the fluxes for the simple, planar wave and the horizontally propagating modal wave show that only a modal wave will tend to form layers, while the simple wave is capable of momentum transport. These results suggest that, in an oceanic region where large-scale internal–inertial waves prevail, the gradient zones in salt and heat will tend to form discontinuities and steps, while the constant-T and S zones will remain unaffected by the instabilities induced by the shear $\overline{U}_z$ associated with wave disturbances that pass through.

The fact that fluxes will also be induced by neutrally stable and damped waves is very significant. The applicability of our analysis to oceanic conditions therefore is of considerable general interest, and the scale of variation of the rotation-and-shear term A in the ocean is a topic considered in the next section.

10. Oceanic applications

The range of variability of the rotation-and-shear term A defined in (6.4) will first be explored to show that values in the range $-10^4 < A < +10^4$ occur in the ocean. We then discuss typical mean-field structure in oceanic regions and sources of excitation which set the initial conditions for instability. This, in turn, will also serve as preparation for the discussion of the probability distribution of the microstructure in §11.

First consider the range of velocity shear found in the ocean. In the Equatorial Undercurrent, a typical minimum vertical shear of the zonal velocity is about -3.2×10^{-2} s^{-1} (above the core), and a maximum shear is about 1.5×10^{-2} s^{-1} (below the core). Because the pycnocline is a natural waveguide, we consider a horizontally propagating wave ($m = 0$). At a latitude of 0.5° S., above the core of the undercurrent, A is -10^4 and smaller for a horizontally propagating wave ($m = 0$) of meridional wavelength 0.5 m and larger. The regime above the core of the undercurrent is generally in the fourth quadrant of the stability diagram. Below the core of the undercurrent, for a horizontal wave with a meridional wavelength of 0.6 m and larger, A is 10^4 and larger. The region below the core of the undercurrent is generally in the third quadrant of the stability diagram. For a horizontally propagating wave ($m = 0$) at 0.5 S. or 0.5 N., $A = 0$ corresponds to a shear of -1.45×10^{-4} s^{-1}.

For tidal-frequency internal waves observed in the tropical Atlantic during the GATE (see Perkins & Van Leer 1977) we estimate typical ranges of shear $\overline{U}_z$ to be Na/H, where N is the maximum Brunt–Väisälä frequency, a is the wave amplitude, and H is the mixed-layer depth. Taking typical values for the subtropical convergence zone with $N = 3 \times 10^{-2}$ s^{-1}, $H = 30$ m and $a = 10$ m, then $U_z \approx 10^{-2}$ s^{-1}. The GATE profiles would generally fall into the third and fourth quadrants of the stability diagram. For the 1.5 km wavelength waves with about 5.5 m amplitude observed during GATE by Proni, Ostapoff & Sellers (1978), in the portion of the tidal wave with $\overline{U}_z = -10^{-2}$ s^{-1}, $A \approx -2 \times 10^{17}$. For a shear of -1.44×10^{-4} s^{-1}, $A \approx 0$ for the same $m = 0$ wave. Since $l \ll 1$ for a long wave and A depends on the difference of a shear term and a constant for $m = 0$, A is sensitive to small changes in a negative shear.

Consider an Arctic regime at about 78 N. For $m = 0$ and $\overline{U}_z \simeq -5 \times 10^{-5}$, a value of $A = -10^4$ corresponds to a meridional wavelength of about 5 m, much larger than in the equatorial case.

At a shear of approximately -3×10^{-5} s^{-1}, $A \approx 0$ for $m = 0$. Thus oceanic regimes typically allow A to range over many orders of magnitude and attain values of $\pm 10^4$ for weak velocity shear.

One oceanic region with large local mean-velocity shear is the equatorial ocean, where the complex large-scale current system produces a region where there are both positive and negative vertical salinity gradients. Consider an internal wave originating well to the south of the equator and travelling northward. As the wave encounters the current shear and salinity stratification, under the right circumstances, the wave will grow in amplitude through the mechanism of instability that we have described. The fluxes induced by the wave will leave a modified stratification, and, as we have shown, these fluxes may enhance vertical gradients of salinity and temperature. In this example, the internal wave acts as an initial disturbance that is amplified through instability. Another role of internal–inertial waves is to provide a local mean shear which induces instabilities of much smaller scale than the waves. In this manner, internal waves can cause small-scale fluxes that modify small-scale stratification.

Other oceanic regions where velocity shear and rotation may enhance mixing are at the north edge of the Antarctic Circumpolar Current and at the meltwater front at the arctic ice edge in summer. For such interfacial layers, more theoretical work is needed, and our analysis may help motivate further work. Spring runoff of coastal fresh water also creates a situation where overstable oscillations may become possible; the change in stratification by possible layer formation is worth exploring further.

The examples show that instability may occur under a wide range of typical oceanic conditions. The applications to particular oceanic problems, because of the sensitivity to wavenumbers and local conditions, will have to be discussed with observational results. Our suggestion that large-scale waves propagating into a region can produce the conditions for local small-scale instability can be pursued further to yield predictions about the probability distribution of microscale salinity and temperature, as will be shown in §11.

11. Probability density

Internal–inertial waves propagating into a region will alter the local shear so that the shear $\overline{U}_z$ may exceed the critical value for instability $\overline{V}_z$ by an amount $\delta(\overline{U}_z - \overline{V}_z)$, where V_z is the shear needed for neutral stability. As we have seen, the consequences

of instability are the generation of increased fluctuations in temperature and salinity, and the occurrence of fluxes that tend to form layers.. We shall assume that the increase in variance in local temperature gradient $\delta[(T_z-\overline{T}_z)^2]$, caused by the occurrence of instability, is proportional to the existing variance times the departure of the velocity shear from the value for neutral stability. As a consequence, we propose the following approximate relation

$$\delta[(T_z-\overline{T}_z)^2] = \gamma(T_z-\overline{T}_z)^2\,\delta(\overline{U}_z-\overline{V}_z). \tag{11.1}$$

Here γ is a constant. This equates the change in perturbation 'energy' to a 'generation' term on the left-hand side. We divide (11.1) by the temperature term on the right-hand side and sum over all shear increments. Approximating the summation by integration yields

$$\ln[(T_z-\overline{T}_z)^2] = \gamma(\overline{U}_z-\overline{V}_z). \tag{11.2}$$

Now if the increments in shear $\delta(\overline{U}_z-\overline{V}_z)$ are independent and possess identical probability distributions, then, according to the central-limit theorem (see Cramer 1946), the distribution function for shear will be a normal distribution function. Consequently, the distribution function for the temperature variance will be lognormal, and the probability density $f_T(T_z)$ for T_z will be of the form

$$f_T(T_z) = (2\pi)^{-\frac{1}{2}}\sigma^{-1}(T_z-\overline{T}_z)^{-2}\exp\left\{-\ln\frac{(T_z-\overline{T}_z)^2}{2\sigma^2}\right\}, \tag{11.3}$$

where σ is the standard deviation.

The condition that the increments $\delta(\overline{U}_z-\overline{V}_z)$ be independent is most likely satisfied by small-scale and relatively high-frequency disturbances compared to internal tides, for example. So lognormal distributions of temperature and salinity gradients should only be expected for the smallest scales of disturbances.

At the smallest scales, one may be able to develop similarity arguments over a range of scales, as was done by Gurvich & Yaglom (1967) in their development of the reasoning of Obukhov (1962) and Komolgorov (1962). Gregg *et al.* (1973) and Elliott & Oakey (1980) find lognormal fluctuations in normalized microscale temperature-gradient variance. The observations of Gregg *et al.* were made in a region below the thermocline where the assumptions of no regular waves are reasonable. The observations by Elliott & Oakey were in the GATE area where there is a strong semidiurnal internal tidal signal, but the pycnocline is very stable and there is a wide spectrum of energetic internal waves. Crawford (1982) finds distributions of both the eddy diffusivity of heat and the rate of dissipation of turbulent energy to be approximately lognormal for data near the equator above the core of the Pacific Equatorial Undercurrent at 150° W.

12. Summary and conclusions

Addition of rotation and shear to the stability analysis of Baines & Gill (1969) leads to the characteristic equation (6.3), which in turn contains the results obtained by them as a special case. Significantly, constant shear has no effect on the stability of double diffusion in the absence of rotation, while rotation has an effect both with and without shear.

The sign of $l\overline{U}_z$, the product of vertical shear and the horizontal wavenumber of the perturbation, in conjunction with mf and lf_{H}, determine the sign and magnitude of the parameter A as indicated in (6.4). The parameter A can assume large positive

and negative values for the range of shears, rotation and wavenumbers likely to be encountered in the ocean. For sufficiently large negative values of A, overstable waves, standing or propagating, can grow faster than salt fingers. For large positive values of A, overstable oscillations are possible over a wide range of unstable density stratification, where, otherwise, simple overturning would occur. We have only considered wave propagation normal to the direction of the shear flow or with rotation alone, and our results cannot be interpreted for different conditions. The results suggest that it may be useful to attempt to solve the more complicated problem of disturbances varying along the flow, as well as normal to it.

One regime where suitable rotation and shear change the instability from salt fingers to overstable waves is where salty, warm water overlays cooler, fresher water, typical of the tropical ocean, as shown, for example, in figure 3. For sufficiently large negative values of A, a wave entering such a region may develop overstability and grow (region IIA) or, as seen in figure 5, change to a direct convective instability (region V). The overstable instability of region II approaches baroclinic instability.

We also have calculated the fluxes of heat, salt, mass and momentum for planar waves traversing a flow of constant shear. Horizontally propagating modal waves will induce fluxes that indicate a trend towards layer formation as a departure from the initial constant gradients. The calculated momentum flux suggests that the fluxes induced by the disturbance can contribute to velocity jet formation and/or sharp shear layers, depending upon the local sign of the mean-velocity shear.

When the shear perturbations caused by large-scale disturbances and those giving rise to instability are statistically independent, and assuming also that these events have identical probability distributions, we predict that the distributions of temperature and salinity gradients will tend towards the lognormal distribution. This result is consistent with observed lognormal distributions for normalized temperature-gradient variance in the ocean.

The analysis shows that overstable oscillatory instability is possible in the tropical ocean pycnocline. Estimates of parameter ranges indicate that overstable waves may be a mechanism for transport of heat, salt, mass and momentum in a considerable part of the world ocean. On the other hand, thermohaline convection will also serve as a damper of internal waves encountering a velocity shear, and transfer energy from the waves to the mean field.

The stability analysis presented can be considered as an extension of the classical arguments used to study the T–S relationship that is used to characterize mixing of water masses.

This research was supported by the NOAA/EPOCS Program and E.M-C. by the Office of Naval Research under contract NO0014-80-C-0273.

REFERENCES

Abramowitz, M. & Stegun, I. A. (eds.) 1965 *Handbook of Mathematical Functions*. Dover.

Baines, P. G. & Gill, A. E. 1963 On thermohaline convection with linear gradients. *J. Fluid Mech.* **37**, 289–306.

Calman, J. 1977 Experiments on high Richardson number instability of a rotating stratified shear flow. *Dyn. Atmos. Oceans* **1**, 277–297.

Cramer, H. 1946 *Mathematical Methods of Statistics*. Princeton University Press.

Crawford, W. R. 1982 Pacific equatorial turbulence. *J. Phys. Oceanogr.* **12**, 1137–1149.

Dowden, J. M. 1972 An equatorial boundary layer. *J. Fluid Mech.* **56**, 193–200.

Duing, W., Ostapoff, F. & Merle, J. (eds.) 1980 *Physical Oceanography of the Tropical Atlantic during GATE*. University of Miami.

ELLIOTT, J. A. & OAKEY, N. S. 1980 Average microstructure levels and vertical diffusion for Phase III, GATE. *Deep-Sea Res.* **26**, (Suppl I), 273–294.

FEDOROV, K. N. 1978 *The Thermohaline Finestructure of the Ocean.* Pergamon.

GANS, R. F. 1975 On the stability of a shear flow in a rotating gas. *J. Fluid Mech.* **68**, 403–412.

GREGG, M. C., COX, C. S. & HACKER, P. W. 1973 Vertical microstructure measurements in the central North Pacific. *J. Phys. Oceanogr.* **3**, 458–469.

GURVICH, A. S. & YAGLOM, A. M. 1967 Breakdown of eddies and probability distributions for small-scale turbulence. *Phys. Fluids Suppl.* **10**, 959–965.

HOLYER, J. 1981 On the collective instability of salt fingers. *J. Fluid Mech.* **110**, 195–207.

HSU, Y. S. 1974 Double diffusive instabilities with and without a weak vertical shear. Ph.D. thesis, Harvard University.

HUPPERT, H. E. & TURNER, J. S. 1981 Double-diffusive convection. *J. Fluid Mech.* **106**, 299–329.

KOLMOGOROV, A. N. 1962 A refinement of previous hypotheses concerning the local structure of turbulence in a viscous incompressible fluid at high Reynolds number. *J. Fluid Mech.* **13**, 82–85.

KOZLOV, V. F. 1967 On the theory of a baroclinic layer at the equator. *Oceanology* **7**, 448–455.

LANDAHL, M. T. 1980 A note on an algebraic instability of inviscid parallel shear flows. *J. Fluid Mech.* **98**, 243–251.

LINDEN, P. F. 1974 Salt fingers in a steady shear flow. *Geophys. Fluid Dyn.* **6**, 1–27.

MCINTYRE, M. E. 1970*a* Diffusive destabilization of the baroclinic circular vortex. *Geophys. Fluid Dyn.* **1**, 19–57.

MCINTYRE, M. E. 1970*b* Role of diffusive overturning in nonlinear axisymmetric convection in a differentially heated rotating annulus. *Geophys. Fluid Dyn.* **1**, 59–89.

MASLOWE, S. A. 1974 Instability of rigidly rotating flows to non-axisymmetric disturbances. *J. Fluid Mech.* **64**, 307–317.

MUNK, W. H. 1966 Abyssal recipes. *Deep-Sea Res.* **13**, 707–730.

OBUKHOV, A. M. 1962 Some specific features of atmospheric turbulence. *J. Fluid Mech.* **13**, 77–81.

PEARLSTEIN, A. J. 1981 Effect of rotation on the stability of a doubly diffusive fluid layer. *J. Fluid Mech.* **103**, 389–412.

PERKINS, H. T. & VAN LEER, J. C. 1977 Simultaneous current–temperature profiles in the Equatorial Countercurrent. *J. Phys. Oceanogr.* **7**, 264–271.

PROCTOR, M. R. E. 1981 Steady subcritical thermohaline convection. *J. Fluid Mech.* **105**, 507–521.

PRONI, J. R., OSTAPOFF, F. & SELLERS, R. L. 1978 Acoustic observations of high-frequency, near-surface internal wave groups in the deep ocean during GATE. *Deep-Sea Res.* **25**, 299–307.

RAYLEIGH, LORD 1878 On the instability of jets. *Proc. Lond. Math. Soc.* **10**, 4–13.

SCHMITT, R. W. & LAMBERT, R. B. 1979 The effects of rotation on salt fingers. *J. Fluid Mech.* **90**, 449–463.

SIEGMANN, W. L. 1974 Evolution of unstable shear layers in a rotating fluid. *J. Fluid Mech.* **64**, 289–305.

STERN, M. E. 1960 The 'salt-fountain' and thermohaline convection. *Tellus* **12**, 172–175.

STERN, M. E. 1969 Collective instability of salt fingers. *J. Fluid Mech.* **35**, 209–218.

STERN, M. E. 1975 *Ocean Circulation Physics.* Academic.

STOMMEL, H. 1962 Examples of mixing and self-stimulated convection on the *S–T* diagram. *Okeanologiya* **2**, 205–209.

SYNGE, J. L. 1938 *Hydrodynamic Stability.* Semi-centennial Publ. Am. Math. Soc., vol. 2 (addresses), pp. 227–269.

TURNER, J. S. & STOMMEL, H. 1964 A new case of convection in the presence of combined vertical salinity and temperature gradients. *Proc. Natl. Acad. Sci.* **52**, 49–53.

VERONIS, G. 1965 On finite-amplitude instability in thermohaline convection. *J. Mar. Res.* **23**, 1–17.

WOODS, J. D. 1968 Wave-induced shear instability in the summer thermocline. *J. Fluid Mech.* **32**, 791–800.